AIAA JOURNAL
Vol. 43, No. 7, July 2005

Influence of Joint Relaxation on Deterministic and Stochastic Panel Flutter

R. A. Ibrahim* and D. M. Beloiu†
Wayne State University, Detroit, Michigan 48202
and
C. L. Pettit‡
U.S. Air Force Research Laboratory, Wright–Patterson Air Force Base, Ohio 45433

The influence of boundary condition relaxation on two-dimensional panel flutter is studied in the absence and presence of random pressure differential and in-plane loading. The boundary-value problem of the panel involves time-dependent boundary conditions that are converted into autonomous form using a special coordinate transformation. The resulting boundary conditions are combined with the governing nonhomogeneous, partial differential equation that includes the influence of the boundary condition relaxation. The relaxation and system nonlinearity are found to have opposite effects on the time evolution of the panel frequency. Furthermore, the damping of the panel exhibits a critical value governed by the relaxation parameter, below which the damping has a destabilizing effect and above the critical value it has stabilizing effect. The influence of random in-plane loading and random pressure differential is estimated using Monte Carlo simulation. Stochastic stability boundaries under random in-plane loading are estimated below and above the critical aerodynamic pressure. Depending on the system damping and dynamic pressure, the time evolution of the panel frequency content can increase or decrease with time as the boundary conditions approach the near simple support case.

Nomenclature

a	=	panel length
a_∞	=	speed of sound, $\sqrt{(\gamma p_\infty/\rho_\infty)}$
$B(\tau)$	=	Brownian motion
c	=	linear viscous damping coefficient
c_p	=	specific heat at constant pressure
c_v	=	specific heat at constant volume
D	=	panel bending stiffness, $Eh^3/[12(1-\nu^2)]$
E	=	Young's modulus
h	=	panel thickness
k	=	slope of relaxation curve at the point of inflection
M	=	Mach number, U_∞/a_∞
m_p	=	panel mass per unit length
$N_{x0}(t)$	=	external in-plane load per unit spanwise length
p_∞	=	undisturbed free gas stream pressure
$q_i(t)$	=	generalized coordinates
U_∞	=	undisturbed gas flow speed
$w(x,t)$	=	panel deflection
$z_i(t)$	=	relaxation parameter, $D/a\alpha_i(t)$
$\alpha_i(t)$	=	torsional stiffnes parameters
γ	=	ratio of specific heat coefficients, C_p/C_v
$\Delta p_0(t)$	=	air pressure across the panel, which consists of static Δp_s and random $\Delta p(t)$ components, $p_0 + \Delta p(t)$
ρ_∞	=	undisturbed free gas stream density
ζ	=	viscous damping factor
$\hat{\zeta}$	=	mass parameter, $\sqrt{(\mu/M)}$
μ	=	air-to-panel mass ratio, $\rho_\infty a/m_p$
ν	=	Poisson's ratio

Received 20 December 2003; revision received 4 May 2004; accepted for publication 7 June 2004.

*Professor, Department of Mechanical Engineering. Associate Fellow AIAA.
†Graduate Research Assistant, Department of Mechanical Engineering.
‡Senior Research Aerospace Engineer, AFRL/VASD; currently Assistant Professor, Aerospace Engineering Department, U.S. Naval Academy, Annapolis, MD 21402. Senior Member AIAA.

Introduction

PANEL flutter under deterministic and stochastic airflow has been extensively studied based on simplified modeling of the structure, aerodynamics, and boundary conditions. The interaction between the panel elastic force and the aerodynamic pressure causes the equations of motion to be non-self adjoint. The aerodynamic pressure fluctuates randomly, and the panel responds as a linear filter. As the flow pressure increases above a critical value, the panel motion changes from a random state to a highly ordered state with increasing amplitude. However, when the panel is subjected to a compressive in-plane load, in addition to the random aerodynamic pressure, the response can undergo complex motions known as chaos.[1,2] According to Fung,[3] a primary difference between the linear theory of panel flutter and experimental results is that experimental observations reveal stochastic forced oscillations as a result of turbulence under which several modes are excited. Another important difference is the influence of nonlinearities of both structural and aerodynamic forces.

Few attempts[4–8] have been made to examine panel flutter and its sensitivity to turbulent pressure fluctuations within the boundary layers. Although Eastep and McIntosh[4] considered structural and aerodynamic nonlinearities, they employed a third-order piston theory to simplify the aerodynamic loading terms in the governing equations. Their deterministic results revealed that the two types of nonlinearities have different consequences on the panel response. The nonlinear interaction between in-plane stresses and transverse deformation provides a stabilizing effect on the panel motion in that it acts to restrain further deformation. The nonlinear aerodynamic loading, on the other hand, has a destabilizing effect in that it acts to increase the panel deformation.

Olson[7] and Vaicaitis et al.[9] utilized Monte Carlo simulation for estimating the response statistics of a panel undergoing large deformation under turbulent boundary-layer pressure. They decomposed the pressure field acting on the panel into three components: the external flow (radiation) pressure, the internal (cavity) pressure, and the random pressure resulting from the boundary-layer fluctuations. The random pressure is represented by a stationary multidimensional Gaussian process, which has a specified cross spectral density. This random process is then simulated by a series of cosine functions with weighted amplitudes, almost evenly random frequencies, and random phase angles that are uniformly distributed between 0

and 2π. The effect of the cavity on panel response was examined for subsonic and supersonic flow regimes. The cavity acts as an air spring resisting the modes that tend to compress the air, thus raising their modal frequencies. For subsonic flow, the response is reduced substantially by the presence of the cavity. However, for supersonic flow flutter occurs at a lower dynamic pressure with a cavity than for the case without a cavity. This is because the first mode frequency is raised by the aerodynamic spring effect producing an earlier coupling between the first and second mode frequencies and thereby induces flutter. The increase of the boundary-layer intensity is found to significantly modify the panel response especially for low air pressure parameter. Other numerical techniques, such as finite element methods, have been used for computing nonlinear flutter characteristics of panels in supersonic flow.[7–9]

Ibrahim et al.[10] and Ibrahim and Orono[11] studied the stochastic flutter of nonlinear panels in supersonic flow subjected to random in-plane loading. They considered two, three, and four modal interactions. The mean square stability boundaries and response moments were determined as functions of the spectral density of in-plane loads, aerodynamic pressure, air-to-structure mass ratio, and structural damping ratios. For equal modal damping coefficients, it was found that the damping stabilizes the panel in the mean square sense. However, a paradoxical effect of the damping was found only for unequal damping coefficients where the effect is nonbeneficial. The nonlinear response statistics were obtained in the time domain, and the steady state revealed that the response process is strictly stationary.

Most of the analyses of panel flutter are based on ideal boundary conditions such as clamped or simply supported edges. However, most fasteners do not satisfy absolute boundary conditions. In addition, fasteners subjected to vibration often lose much of their preload; this is known as relaxation. First there is a slow loss of preload caused by some of the relaxation mechanisms. Vibration increases relaxation because wear and hammering take place during vibration. Vibration-induced loosening and relaxation effects cause time-dependent boundary conditions and depend on the level of structural vibration. Recently, Ibrahim and Pettit[12] presented an extensive review of dynamic problems associated with joint relaxation and uncertainties.

However, a limited number of studies have considered the influence of uncertainties in aeroelastic structures and their boundary conditions. For example, Poiron[13] introduced uncertainties in analyzing the flutter characteristics of aircraft models and used a first-order perturbation method and Monte Carlo simulation to determine the flutter probability for different values of flow speeds and mass parameters. The effect of uncertainty in the boundary conditions, combined with the variability of material properties, on nonlinear panel aeroelastic response was studied by Lindsley et al.[14,15] Pinned and fixed boundary conditions were modeled as limiting cases of rotational springs on the boundary, which possess zero and infinite stiffness, respectively. Accordingly, rotational spring stiffness was used to parameterize the boundary conditions. Parametric uncertainty was examined by modeling variability in Young's modulus and the boundary conditions. Variability in the boundary conditions was restricted to a single value along the plate boundary edges for each realization. It was reported that for values of dynamic pressure in the deterministic limit-cycle oscillation range the variability in the boundary conditions affects the panel deflection in an essentially linear manner. However, for values in the neighborhood of bifurcation point the relationship is nonlinear. Variation in the boundary conditions results in a softening effect of the clamped panel and thus induces an increase in the amplitude of plate oscillations.

Although Lindsley et al.[14,15] considered the effect of variability in boundary rotational stiffness, none of the studies just cited included the influence of time-dependent boundary conditions on the flutter characteristics of aeroelastic structures. Relaxation, or the loss of preload in mechanical joints, is a common problem in vibrating structures that must be addressed to ensure that the structure will perform satisfactorily throughout its expected life. The present work is an extension of the work of Ibrahim et al.[10,11,16] and Qiao et al.[17] to examine the influence of relaxation of boundary conditions on the panel flutter characteristics such as modal natural frequencies and limit-cycle amplitudes and stochastic stability under random in-plane loading.

Nonlinear panel flutter with relaxation in the boundary conditions is studied based on a phenomenological model of joint preload relaxation and random aerodynamic pressure superposed on piston theory loads. The random pressure is characterized by a power spectral density for which empirical expressions can be used, or an assumed Markov field can be introduced. The use of empirical expressions requires numerical simulation of the equations of motion, and the Markov field approximation yields a set of differential equations for the response moments. In view of the nonstationarity imposed by joint relaxation and the multidimensionality of the problem, it is not possible to obtain a closed-form solution for the panel response statistics. Instead, we will resort to Monte Carlo simulation.

The conventional boundary-value problem of the panel involves time-dependent boundary conditions that are converted to an autonomous form using a special coordinate transformation introduced by Qiao et al.[17] The resulting boundary conditions are combined with the governing nonhomogeneous, partial differential equation that includes the influence of the boundary condition relaxation. The analysis is restricted to two-mode interaction through a projection of the governing equations onto the first two baseline structural modes. Results include the influence of boundary condition relaxation on the panel modal frequencies, limit-cycle amplitudes in the time and frequency domains, and mean square stability. Ibrahim et al.[16] showed that when only deterministic aerodynamics are included this model indicates that the relaxation and system nonlinearity have opposite effects on the frequency evolution of the panel. In this paper, these observations will be extended by examining the time- and frequency-domain dependence of the panel's mean square response on the pressure differential spectral density and aerodynamic pressure. The frequency content of the panel's response in the first two modes will be examined through the spectrogram, which will reveal the relaxation-induced nonstationarity of the panel flutter.

Analysis

Consider a two-dimensional panel exposed to supersonic gas flow as shown in Fig. 1. Based on the quasi-steady, supersonic theory, the deflection of a two-dimensional panel undergoing cylindrical bending is caused by the interaction of inertia, elastic, and aerodynamic forces. The governing equation of motion can be developed using Hamilton's principle. To estimate the work done by aerodynamic loading, the pressure on the panel is estimated by using piston theory with quadratic nonlinearity:

$$\Delta p = p - p_\infty = \frac{\rho_\infty U_\infty^2}{M}\left(\frac{\partial w}{\partial x} + \frac{1}{U_\infty}\frac{\partial w}{\partial t}\right) + \rho_\infty \frac{(\gamma+1)}{4}\left[\left(\frac{\partial w}{\partial t}\right)^2 + 2U_\infty \frac{\partial w}{\partial t}\frac{\partial w}{\partial x} + U_\infty^2\left(\frac{\partial w}{\partial x}\right)^2\right] \quad (1)$$

Accurate representation of the pressure is to include cubic nonlinearity in the preceding expression. However, because of boundary condition relaxation, the analysis will be too complicated, and the effect of cubic nonlinearity will be considered in a separate study.

The governing nonlinear equation of motion for the panel is developed using Hamilton's principle, which yields

$$m_p \frac{\partial^2 w}{\partial t^2} + D\left(1 + c\frac{\partial}{\partial t}\right)\frac{\partial^4 w}{\partial x^4} - \left[N_{x0}(t) + \frac{Eh}{2a}\int_0^a \left(\frac{\partial w}{\partial x}\right)^2 \mathrm{d}x\right]\frac{\partial^2 w}{\partial x^2} + \frac{\rho_\infty U_\infty^2}{M}\left(\frac{\partial w}{\partial x} + \frac{1}{U_\infty}\frac{\partial w}{\partial t}\right) + \rho_\infty \frac{(\gamma+1)}{4} \times \left[\left(\frac{\partial w}{\partial t}\right)^2 + 2U_\infty \frac{\partial w}{\partial t}\frac{\partial w}{\partial x} + U_\infty^2\left(\frac{\partial w}{\partial x}\right)^2\right] = \Delta p_0(t) \quad (2)$$

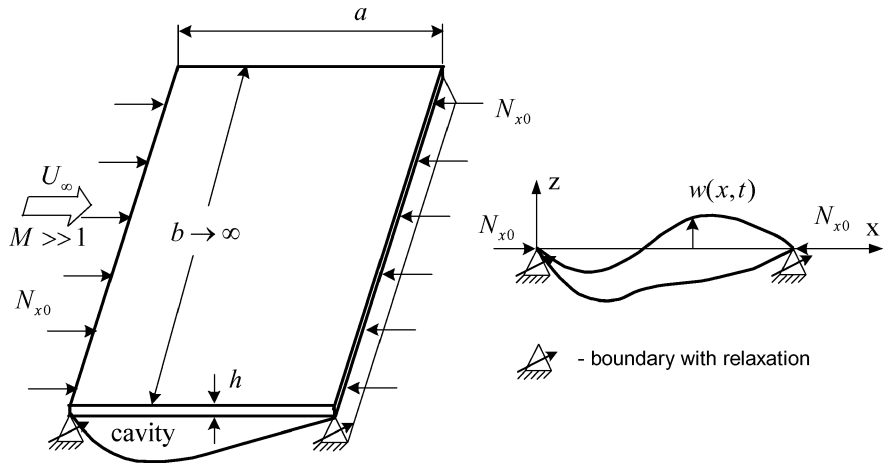

Fig. 1 Schematic diagram of a two-dimensional panel exposed to supersonic flow supported on boundaries with relaxation.

$\Delta p_0(t) = p_0 + \Delta p(t)$ is the air pressure across the panel, which consists of static p_s and random $\Delta p(t)$, components. $N_{x0}(t) = N_{x0} + N_x(t)$ is the external in-plane load per unit spanwise length and can be random in time. Equation (2) is subject to the boundary conditions

$$D\frac{\partial^2 w(0,t)}{\partial x^2} - \alpha_1(t)\frac{\partial w(0,t)}{\partial x} = 0 \tag{3a}$$

$$w(0,t) = 0 \tag{3b}$$

$$D\frac{\partial^2 w(a,t)}{\partial x^2} + \alpha_2(t)\frac{\partial w(a,t)}{\partial x} = 0 \tag{3c}$$

$$w(a,t) = 0 \tag{3d}$$

where $\alpha_1(t)$ and $\alpha_2(t)$ measure the end slopes and represent torsional stiffness parameters such that for $\alpha_1(t) = \alpha_1(t) = \infty$ we have the case of purely clamped–clamped panel. On the other hand, $\alpha_1(t) = \alpha_1(t) = 0$ corresponds to the case of simple supports. In real situations, both $\alpha_1(t)$ and $\alpha_2(t)$ do not assume these extreme cases, and their values are very large for clamped supports or very small for simple supports. In the dynamic case boundary conditions (3a) and (3c) are nonautonomous. To convert these conditions into an autonomous form, we introduce the following transformation of the response coordinate:

$$w(x,t) = \left[\left(\frac{x}{a}\right)^2 + 2g_1(z_1,z_2)\frac{x}{a} + g_2(z_1,z_2)\right]u(x,t)$$

$$= \varphi(x; z_1, z_2)u(x,t) \tag{4}$$

where the dimensionless parameter $z_i(t) = D/a\alpha_i(t)$, $i = 1,2$, represents the ratio of the bending rigidity to the torsional stiffness of the joints. The functions $g_1(z_1, z_2)$ and $g_2(z_1, z_2)$ are chosen to render the boundary conditions autonomous for the new coordinate $u(x,t)$. Possible expressions of these functions[17] are

$$g_1(z_1,z_2) = -\frac{1+4z_2}{2(1+2z_1+2z_2)}$$

$$g_2(z_1,z_2) = -\frac{2z_1(1+4z_2)}{1+2z_1+2z_2} \tag{5}$$

In this case, the boundary conditions (3) become

$$\frac{\partial^2 u(0,t)}{\partial x^2} = \frac{\partial^2 u(a,t)}{\partial x^2} = 0, \qquad u(0,t) = u(a,t) = 0 \tag{6}$$

Introducing the nondimensional parameters

$$\tau = t\sqrt{\frac{D}{m_p a^4}}, \qquad \bar{w} = \frac{w}{h}, \qquad \bar{x} = \frac{x}{a}, \qquad \lambda = \frac{\rho_\infty U_\infty^2 a^3}{MD}$$

$$\mu = \frac{\rho_\infty a}{m_p}, \qquad \zeta = \frac{c}{a^2}\sqrt{\frac{D}{m_p}}, \qquad \bar{N}_{x0}(\tau) = N_{x0}(t)\frac{a^2}{D}$$

$$\Delta\bar{p}_0(\tau) = \Delta p_0(t)\frac{a^4}{Dh}, \qquad B_1 = 6(1-\nu^2)$$

$$B_2 = \frac{\gamma+1}{4}\frac{\rho h}{m_p}, \qquad B_3 = \frac{\gamma+1}{2\sqrt{m_p D}}\rho_\infty U_\infty a h$$

$$B_3 = \frac{\gamma+1}{2}\rho_\infty U_\infty^2 \frac{a^2 h}{D}, \qquad \bar{u} = \frac{u}{h}$$

$$\bar{\varphi} = [\bar{x}^2 + 2g_1(z_1,z_2)\bar{x} + g_2(z_1,z_2)], \qquad \hat{\zeta} = \sqrt{\frac{\mu}{M}}$$

Eq. (2) becomes

$$\frac{\partial^2(\bar{\varphi}\bar{u})}{\partial\tau^2} + \left(1 + \zeta\frac{\partial}{\partial\tau}\right)\frac{\partial^4(\bar{\varphi}\bar{u})}{\partial\bar{x}^4}$$

$$-\left\{\bar{N}_{x0}(\tau) + B_1\int_0^1\left[\frac{\partial(\bar{\varphi}\bar{u})}{\partial\bar{x}}\right]^2 \mathrm{d}\bar{x}\right\}\frac{\partial^2(\bar{\varphi}\bar{u})}{\partial\bar{x}^2}$$

$$+\lambda\frac{\partial(\bar{\varphi}\bar{u})}{\partial\bar{x}} + \hat{\zeta}\sqrt{\lambda}\frac{\partial(\bar{\varphi}\bar{u})}{\partial\tau} + B_2\left[\frac{\partial(\bar{\varphi}\bar{u})}{\partial\tau}\right]^2$$

$$+B_3\frac{\partial(\bar{\varphi}\bar{u})}{\partial\tau}\frac{\partial(\bar{\varphi}\bar{u})}{(\partial\bar{x})} + B_4\left[\frac{\partial(\bar{\varphi}\bar{u})}{\partial\bar{x}}\right]^2 = \bar{p}_0(\tau) \tag{7}$$

The preload relaxation process is phenomenologically modeled based on experimental results.[18] First, it is assumed that the torsional stiffness parameters are functions of the number of vibration cycles $n = n(\tau)$:

$$\bar{\alpha}_i(n) = \frac{a\alpha_i(n)}{D} = \frac{1}{z_i(n)} \tag{8}$$

where the overbar denotes a dimensionless parameter. An explicit analytical expression for the parameters $\bar{\alpha}_i(n)$ can be obtained from experimental records.[18] These experimental measurements revealed the trend of the relaxation process as a slow drop between an original and an asymptotic value of the joint stiffness. An appropriate

elementary function that emulates this behavior can be selected in the form

$$\bar{\alpha}(n) = A + B\tanh[-k(n-n_c)] \tag{9}$$

where the subscript i has been dropped and n_c is a critical number of cycles, indicating the location of the inflection point with respect to the origin $n=0$. The parameter k is associated with the slope of the curve at point $n=n_c$. The constants A and B are determined from the initial and final values of the stiffness parameter by solving the two algebraic equations

$$\bar{\alpha}(0) = A + B\tanh[kn_c] \tag{10a}$$

$$\bar{\alpha}(\infty) = A + B \tag{10b}$$

Solving for A and B and substituting in relation (9) gives

$$\bar{\alpha}(n) = \bar{\alpha}(\infty) + [\bar{\alpha}(0) - \bar{\alpha}(\infty)]\left\{\frac{1+\tanh[-k(n-n_c)]}{1+\tanh(kn_c)}\right\} \tag{11}$$

The parameters $\bar{\alpha}(0)$ and $\bar{\alpha}(\infty)$ are obtained from the experimental curve. The slope parameter k can be found by taking the derivative of Eq. (11) with respect to n, that is,

$$k = \frac{\partial\bar{\alpha}(n)/\partial n|_{n_c}}{[\bar{\alpha}(\infty) - \bar{\alpha}(0)]}[1+\tanh(kn_c)] \tag{12}$$

One can write an expression for $z(\tau)$ by using relations (8) and (11) in the form

$$z(\tau) = Z_0 Z_\infty\left\{Z_0 - (Z_0 - Z_\infty)\frac{1+\tanh[-\chi(\tau-\tau_c)]}{1+\tanh(\chi\tau_c)}\right\}^{-1} \tag{13}$$

where $Z_0 = z(0)$; $Z_\infty = z(\infty)$; $\chi = \langle\varpi\rangle/2\pi k$, where $\langle\varpi\rangle$ is the mean value of the response frequency and can be taken as the center frequency. The phenomenological representation given by Eq. (13) can be used for any initial preload and will cause the panel to experience nonstationary behavior.

Galerkin's method is applied to discretize Eq. (7) by assuming the general solution in the form

$$\bar{u}(\bar{x},\tau) = \sum_{n=1}^{N} q_n(\tau)\sin n\pi\bar{x} \tag{14}$$

where N is the total number of modes and $q_n(\tau)$ are the generalized coordinates. For the present study, we consider two-mode interaction, that is, $N=2$. Furthermore, it is assumed that $z_1 = z_2 = z/2$, which makes the boundary stiffness values symmetric. The following two nonlinear ordinary differential equations are obtained:

$$\begin{aligned} &q_1''(\tau) + \left(\zeta a_{11} + \hat{\zeta}\sqrt{\lambda}\right)q_1'(\tau) + [a_{12}\bar{N}_{x0}(\tau) + a_{13}]q_1(\tau) \\ &\quad + (a_{14}\lambda + a_{15})q_2(\tau) + B_2 b_{11} q_1'(\tau)^2 \\ &\quad + B_2 b_{12} q_2'(\tau)^2 + B_3 b_{13} q_1'(\tau)q_2(\tau) + B_3 b_{14} q_1(\tau)q_2'(\tau) \\ &\quad + B_1 b_{15} q_1(\tau)^3 + B_1 b_{16} q_1(\tau)q_2(\tau)^2 + B_4 b_{17} q_1(\tau)^2 \\ &\quad + B_4 b_{18} q_2(\tau)^2 = [12\bar{p}_0(\tau)/\pi][1/c_0(\tau)] \end{aligned} \tag{15a}$$

$$\begin{aligned} &q_2''(\tau) + \left(\zeta a_{21} + \hat{\zeta}\sqrt{\lambda}\right)q_2'(\tau) + [a_{22}\bar{N}_{x0}(\tau) + a_{23}]q_2(\tau) \\ &\quad + (a_{24}\lambda + a_{25})q_1(\tau) + B_2 b_{21} q_1'(\tau)q_2'(\tau) + B_3 b_{22} q_1'(\tau)q_1(\tau) \\ &\quad + B_3 b_{23} q_2(\tau)q_2'(\tau) + B_4 b_{42} q_1(\tau)q_2(\tau) \\ &\quad + B_1 b_{25} q_2(\tau)^3 + B_1 b_{26} q_1(\tau)^2 q_2(\tau) = 0 \end{aligned} \tag{15b}$$

where a prime denotes differentiation with respect to the nondimensional time parameter τ, the coefficients a_{ij} and b_{ij} are functions of the relaxation parameter z, which is time dependent, and

$$a_{11} = \frac{\pi^4[51+\pi^2(1+6z)]}{3+\pi^2(1+6z)}, \qquad a_{12} = \pi^2, \qquad a_{13} = a_{11}$$

$$a_{14} = -\frac{16(26+9\pi^2 z)}{9[3+\pi^2(1+6z)]}, \qquad a_{15} = \frac{64}{3[3+\pi^2(1+6z)]}$$

$$b_{11} = -\frac{16[728+27\pi^4 z^2+60\pi^2(-1+2z)]}{27\pi^3[3+\pi^3(1+6z)]}$$

$$b_{12} = -\frac{64[380{,}408+16{,}875\pi^4 z^2+32{,}100\pi^2(-1+2z)]}{84{,}375\pi^3[3+\pi^3(1+6z)]}$$

$$b_{13} = \frac{45+30\pi^2 z+\pi^4(1+10z+30z^2)}{5\pi[3+\pi^2(1+6z)]}$$

$$b_{14} = -\frac{1395+840\pi^2 z+16\pi^4(1+10z+30z^2)}{160\pi[3+\pi^2(1+6z)]}$$

$$b_{15} = \frac{1}{60}[-15+10\pi^2(1+3z)+\pi^4(1+10z+30z^2)]$$

$$b_{16} = -\frac{1}{16}+\frac{1}{6}\pi^2(1+3z)+\pi^4\left(\frac{1}{15}+\frac{2z}{3}+2z^2\right)$$

$$b_{17} = -\frac{8[488+27\pi^4 z^2+12\pi^2(-2+13z)]}{27\pi[3+\pi^2(1+6z)]}$$

$$b_{18} = -\frac{32[2{,}783{,}096+118{,}125\pi^4 z^2+300\pi^2(-734+1693z)]}{84{,}375\pi[3+\pi^2(1+6z)]}$$

$$c_0(\tau) = -\frac{3+\pi^2+6\pi^2 z}{12\pi^2}$$

$$a_{21} = 16a_{11}, \qquad a_{22} = 4a_{12}, \qquad a_{23} = a_{21}$$

$$a_{24} = \frac{64(14+9\pi^2 z)}{9[3+4\pi^2(1+6z)]}, \qquad a_{25} = 4a_{15}$$

$$b_{21} = 8b_{12}, \qquad b_{22} = -4b_{14}$$

$$b_{23} = -\frac{32(5+3\pi^2 z)}{9\pi[3+4\pi^2(1+6z)]}$$

$$b_{24} = -\frac{256[127{,}688+16{,}875\pi^4 z^2+300\pi^2(-2+229z)]}{84{,}375\pi[3+4\pi^2(1+6z)]}$$

$$b_{25} = -\frac{1}{4}+\pi^2\left(\frac{2}{3}+2z\right)+\pi^4\left(\frac{4}{15}+\frac{8z}{3}+8z^2\right)$$

$$b_{26} = -1+\pi^2\left(\frac{2}{3}+2z\right)+\pi^4\left(\frac{1}{15}+\frac{2z}{3}+2z^2\right) \tag{16}$$

Equations (15) are solved numerically in the time domain for a typical relaxation curve. The resulting solution is given in terms of the transformed response $\bar{u}$, or rather in terms of its modal coordinates q_i, $i=1,2$. One should estimate the panel modal response in terms of its physical generalized coordinate:

$$\bar{w}(\bar{x},\tau) = \varphi(\bar{x})\bar{u}(\bar{x},\tau), \qquad \bar{w}(\bar{x},\tau) = \sum_{n=1}^{N}\hat{q}_n(\tau)\sin n\pi\bar{x} \tag{17}$$

where $\bar{\varphi} = [\bar{x}^2 + 2g_1(z_1,z_2)\bar{x} + g_2(z_1,z_2)]$ and g_i are given by Eq. (5). The relationship between the physical coordinates $\hat{q}_n(\tau)$

and the generalized transformed coordinates $q_n(\tau)$ is

$$\sum_{n=1}^{N} \hat{q}_n(\tau) \sin n\pi\bar{x} = [\bar{x}^2 + 2g_1(z)\bar{x} + g_2(z)] \sum_{n=1}^{N} q_n(\tau) \sin n\pi\bar{x} \tag{18}$$

Multiplying both sides of Eq. (18) by $\sin m\pi\bar{x}$, $m = 1, 2$, and integrating both sides,

$$\int_0^1 \left[\sum_{n=1}^{N} \hat{q}_n(\tau) \sin n\pi\bar{x} \sin m\pi\bar{x} \right] \mathrm{d}x = \int_0^1 \left\{ [\bar{x}^2 + 2g_1(z)\bar{x} + g_2(z)] \sum_{n=1}^{N} q_n(\tau) \sin n\pi\bar{x} \sin m\pi\bar{x} \right\} \mathrm{d}x \tag{19}$$

gives the relation between coordinates

$$\begin{Bmatrix} \hat{q}_1(\tau) \\ \hat{q}_2(\tau) \end{Bmatrix} = \begin{bmatrix} T_{11}(z) & T_{12}(z) \\ T_{21}(z) & T_{22}(z) \end{bmatrix} \begin{Bmatrix} q_1(\tau) \\ q_2(\tau) \end{Bmatrix} \tag{20}$$

where

$$T_{11}(z) = T_{22}(z) = -\frac{\pi^2}{2 + \pi^2 z}, \qquad T_{12}(z) = T_{21}(z) = 0 \tag{21}$$

Relation (20) gives

$$\hat{q}_1(\tau) = -\frac{\pi^2}{2 + \pi^2 z} q_1(\tau), \qquad \hat{q}_2(\tau) = -\frac{\pi^2}{2 + \pi^2 z} q_2(\tau) \tag{22}$$

Deterministic Analysis

The deterministic analysis is carried out based on constant values of in-plane force $\bar{N}_{x0}(\tau) = \bar{N}_{x0}$ and constant external pressure $\bar{p}_0(\tau) = \bar{p}_0$. The influence of boundary conditions relaxation on the panel eigenvalues can be examined by dropping the nonlinear and nonhomogeneous terms from modal equations (15). The dependence of the real and imaginary parts of the modal eigenvalues on the dynamic pressure λ and relaxation parameter z is shown in Figs. 2a and 2b by three-dimensional diagrams for damping parameter $\zeta = 0.0$, mass parameter $\hat{\zeta} = 0.0$, and static axial load parameter $\bar{N}_{x0} = 0$. It is seen that the real parts are zero up to a critical value of the dynamic pressure, depending on the value of the relaxation parameter z, above which one becomes negative and the other positive indicating the occurrence of panel flutter. Note that the value $z = 0$ corresponds to clamped–clamped panel, and the corresponding critical dynamic pressure is greater than any case with $z > 0$. For nonzero positive damping and mass ratio, both real parts are negative up to a critical dynamic pressure value above which one remains negative and the other crosses the λ axis, and then assumes positive value. Figure 2b shows the imaginary part, which represents the natural frequencies of the two modes. The dependence of the real part on the dynamic pressure for different values of relaxation parameter is shown in Fig. 3a, where the crossing to positive values signals the occurrence of flutter. As expected, as the panel nears clamped boundary conditions the occurrence of flutter is delayed for relatively higher values of dynamic pressure. The dependence of the natural frequencies of the first and second modes on the relaxation parameter z is shown in Figs. 3a and 3b for different values of dynamic pressure parameter. For a fixed value of dynamic pressure, the first-mode natural frequency decreases with the relaxation parameter but increases with dynamic pressure as shown in Fig. 3a. On the other hand, the natural frequency of the second mode (Fig. 3b) decreases with the relaxation parameter and with dynamic pressure as well. Note that the second mode experiences a drop in its natural frequency up to near the critical dynamic pressure above which its value increases again.

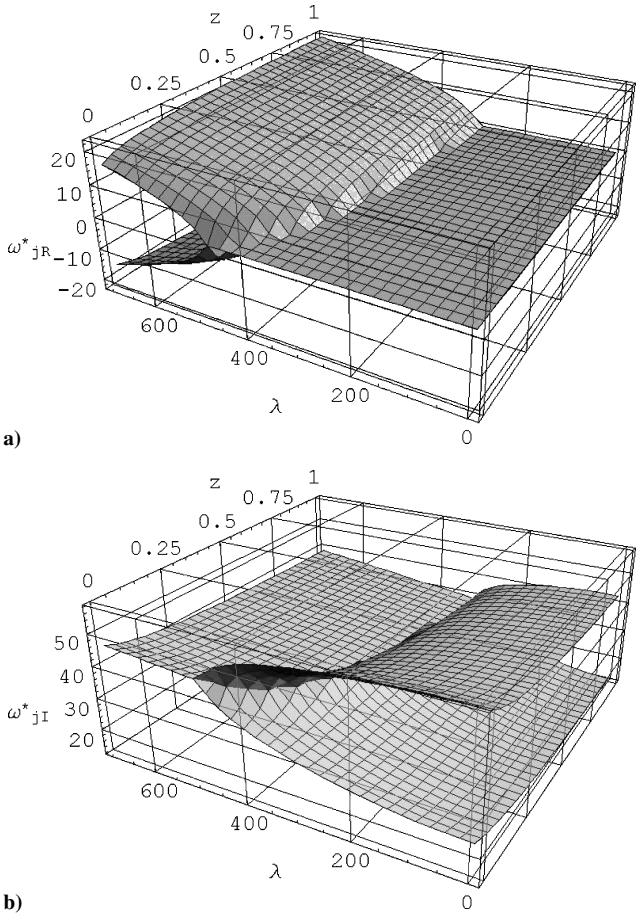

Fig. 2 Dependence of real and imaginary parts of the panel natural frequency on dynamic pressure and boundary condition relaxation parameter z for $\zeta = 0$, $\hat{\zeta} = 0$, $N_0 = 0$: a) real and b) imaginary parts.

The dependence of the critical value of aerodynamic pressure on the in-plane static load $\bar{N}_{x0}$, damping ratio ζ, and relaxation parameter z, is shown in Figs. 4–6, respectively. These figures represent the boundaries of panel flutter for different parameters of relaxation parameter as shown in Figs. 4 and 5. As expected, the compression in-plane loading results in a reduction of the critical flutter speed. The clamped panel ($z \ll 1$) requires more in-plane compression load to reach its flutter speed. Figure 5 shows the dependence of flutter speed on the damping parameter ζ. For a given relaxation parameter, there is a critical damping ratio ζ_{cr} above which the damping becomes beneficial and the critical speed increases with the damping. For $\zeta < \zeta_{\mathrm{cr}}$ the damping is nonbeneficial and results in a reduction the flutter speed. The critical damping ratio is determined by setting $\mathrm{d}\lambda/\mathrm{d}\zeta = 0$, and the dashed curve in Fig. 5 shows the locus of the critical damping ratio. For equal modal viscous damping coefficients, the damping is known to stabilize the panel. However, as shown in Ibrahim et al.,[10] and the cited references therein, unequal modal damping coefficients result in a paradoxical effect. Figure 6 shows the dependence of the flutter speed on the relaxation parameter for different values of static in-plane loading. The destabilizing effect of damping is shown in Fig. 7, where the instability region increases as the damping increases then decreases depending on the relaxation parameter.

Figure 8 shows the dependence of the limit-cycle-oscillation (LCO) amplitude of the first mode on the dynamic pressure for different discrete values of the relaxation parameter z in the form of supercritical bifurcation. The two ideal cases of purely simple–simple and clamped–clamped boundary conditions are plotted by solid curves. Note that the relaxation results in moving the bifurcation point to lower values of dynamic pressure. Figure 9 shows

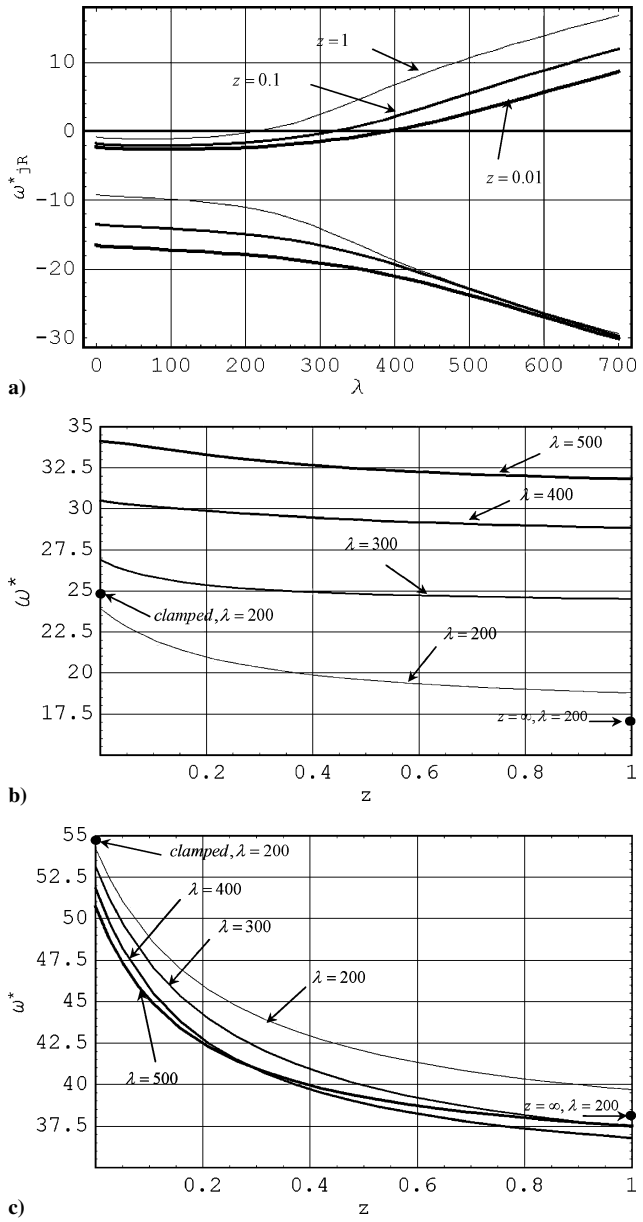

Fig. 3 Dependence of modal natural frequencies on the relaxation parameter for different values of dynamic pressure parameter λ and for $\zeta = 0.01$, $\hat{\zeta} = 0.1$, $N_0 = 0$: a) two-dimensional representation of the real parts, b) first mode, and c) second mode.

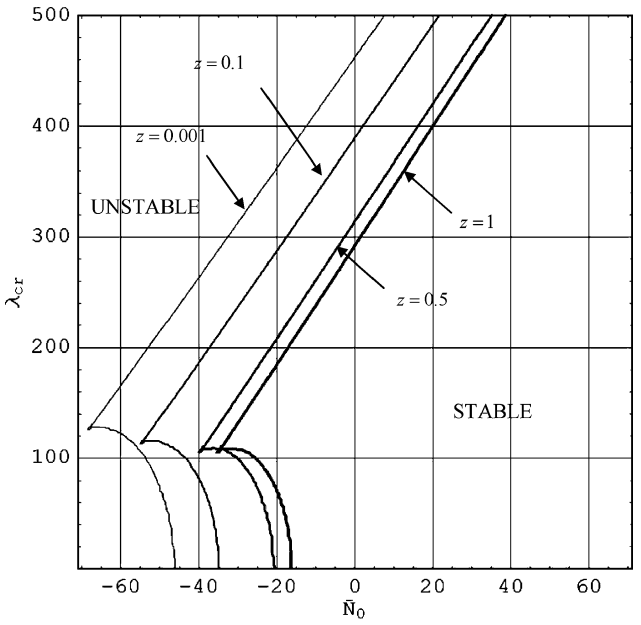

Fig. 4 Boundaries of panel flutter on the $\lambda - \bar{N}_0$ plane for different values of relaxation parameter and for $\zeta = 0.001$, $\hat{\zeta} = 0.1$.

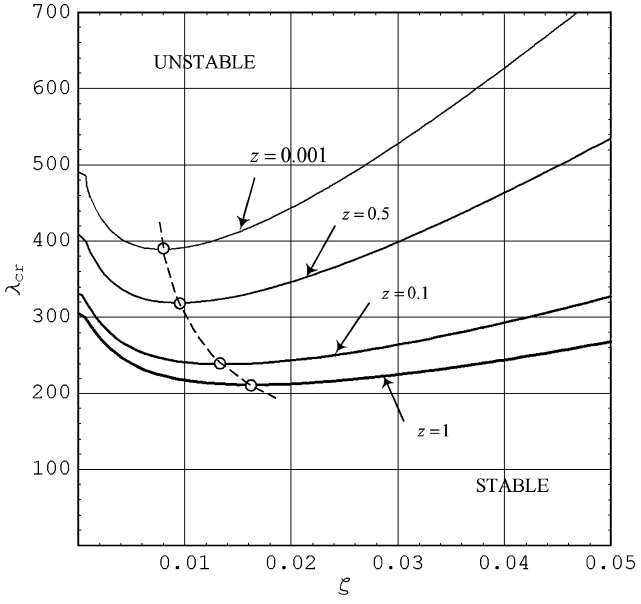

Fig. 5 Boundaries of panel flutter on the $\lambda - \zeta$ plane for different values of relaxation parameter and for $\bar{N}_0 = 0.0$, $\hat{\zeta} = 0.1$: – – –, the critical damping ratio that separates stabilizing and destabilizing damping effects.

the dependence of time evolution of the LCO amplitude on the dynamic pressure in three-dimensional plots for $\zeta = 0.001$, $\hat{\zeta} = 0.1$, and $\bar{N}_{x0} = 0$. Note the time axis gives also a measure of the relaxation parameter.

The panel experiences flutter above the critical value of dynamic pressure depending on the relaxation parameter. The inclusion of nonlinearities in Eq. (15) causes the flutter to achieve a limit cycle. However, because of relaxation time history record shown in Fig. 10a, the panel response experiences nonstationary limit-cycle oscillations as the dynamic pressure exceeds its critical value. For example, Fig. 10b shows the panel first-mode time-history response record for dynamic pressure $\lambda = 260 < \lambda_{cr}$, where λ_{cr} corresponds to the critical dynamic pressure for absolute clamped–clamped panel. It is seen that the two modes remain stable until the relaxation brought them into near simply support condition at which they start to experience LCO. For dynamic pressure values that exceed the critical value of the clamped condition, the panel experiences unsteady LCO during the relaxation process as shown in Fig. 10c. It is seen that the amplitude of LCO increases with time as the panel boundary conditions change from clamped to near simple support conditions. In all time-history records the LCO does not have zero mean value because of the pressure differential.

The fast Fourier transform (FFT) and spectrogram plots of the first mode shown in Figs. 11a–11c for different values of dynamic pressure reveal that the frequency content includes one spike at zero frequency, because of the static pressure differential, and another band-limited response covering a frequency band whose band depends on the dynamic pressure. This frequency band reflects the time variation of the panel frequency with time. This is demonstrated by inspecting the corresponding spectrograms. The time evolutions of the frequency content represented by the spectrograms in Figs. 10b and 10c demonstrate the correlation between the variation of the frequency with the relaxation process and dynamic pressure. For the cases $\lambda = 500$, $\zeta = 0.01$, and $\lambda = 600$, $\zeta = 0.03$, the response frequency increases as the joint passes through relaxation. On the one hand, the relaxation results in a reduction of the panel natural

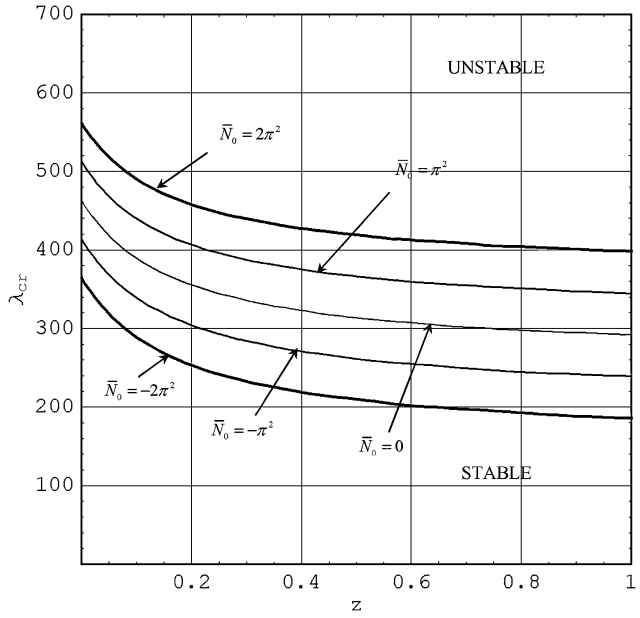

Fig. 6 Boundaries of panel flutter on the $\lambda - z$ plane for different values of in-plane load $\bar{N}_0$ and for $\zeta = 0.001$, $\hat{\zeta} = 0.1$.

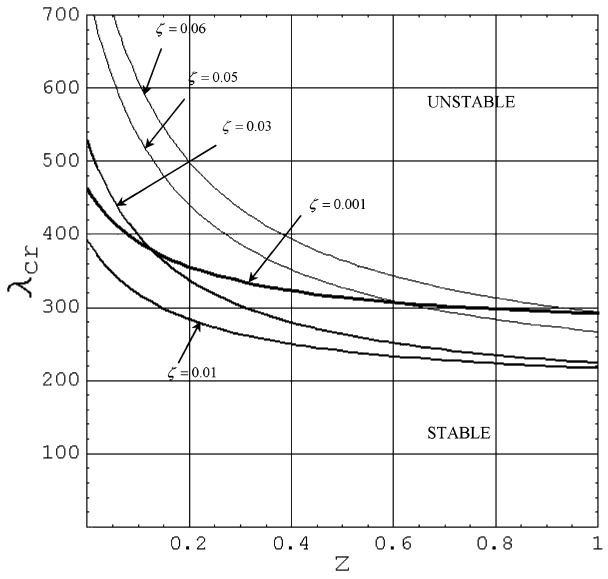

Fig. 7 Boundaries of panel flutter on the $\lambda - z$ plane for different values of damping factor showing the reversal effect of damping for $\hat{\zeta} = 0.1$, $\bar{N}_0 = 0$.

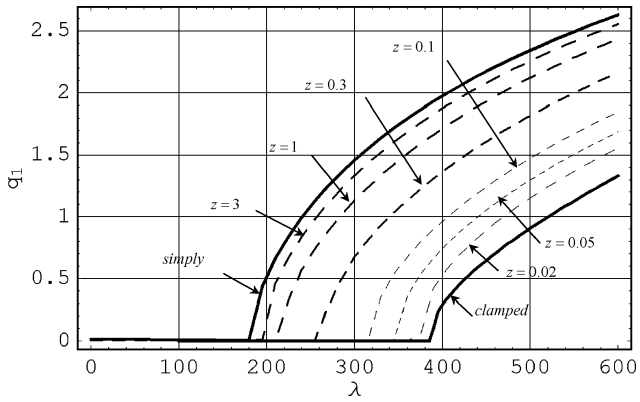

Fig. 8 Bifurcation diagram of the first mode for different values of relaxation parameter showing the absolute cases of simply–simply and clamped–clamped panels for $\zeta = 0.001$, $\hat{\zeta} = 0.1$, $\bar{P}_0 = 1$, and $\bar{N}_0 = 0$.

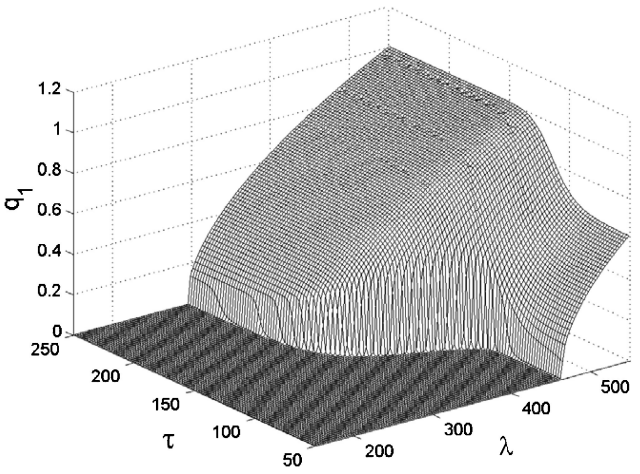

Fig. 9 Three-dimensional plot of the first-mode amplitude time evolution and its dependence on dynamic pressure for $\zeta = 0.001$, $\hat{\zeta} = 0.1$, $\bar{P}_0 = 1$, and $\bar{N}_0 = 0$.

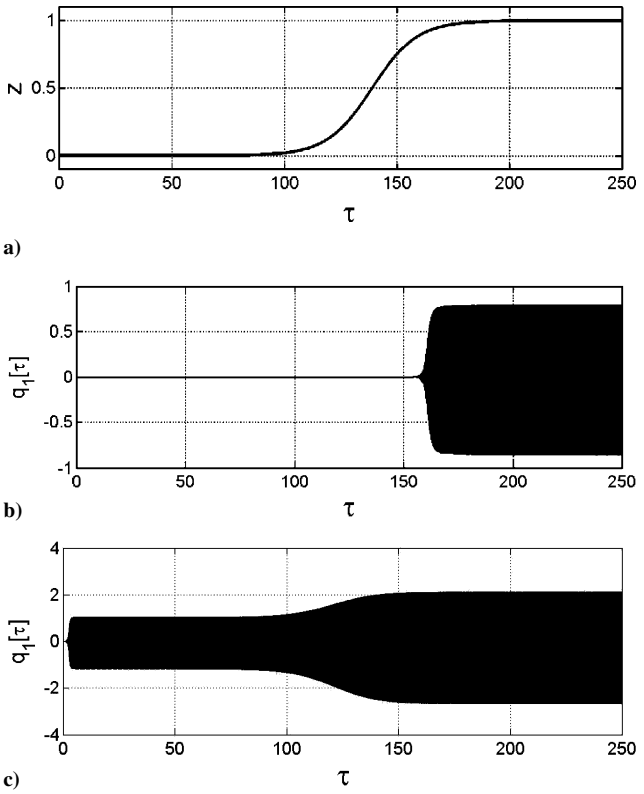

Fig. 10 Time-history records of a) relaxation parameter z and b) and c) first-mode amplitudes for $\bar{P}_0 = 1$, where b) $\lambda = 260 < \lambda_{cr}$, $\zeta = 0.01$, $\hat{\zeta} = 0.1$, $\bar{N}_0 = 0$; and c) $\lambda = 500 > \lambda_{cr}$, $\zeta = 0.001$, $\hat{\zeta} = 0.1$, $\bar{N}_0 = 0$.

frequency. On the other hand, the nonlinearity of the panel is of a hard spring characteristics and causes an increase in the frequency with the LCO amplitude. It appears that the nonlinearity overcomes the softening effect of relaxation for the two cases of Figs. 11a and 11c. For the case $\lambda = 500$, $\zeta = 0.001$ shown in Fig. 11b, the relaxation is almost in balance with the nonlinearity, and the frequency content exhibits a very slight drop over time.

Random Analysis

The panel is exposed to turbulent pressure fluctuations within the boundary layers. These fluctuations are random, and the pressure is characterized by a power spectral density for which empirical expressions can be used, or an assumed Markov field can be introduced. As mentioned in the Introduction, experimental observations reveal

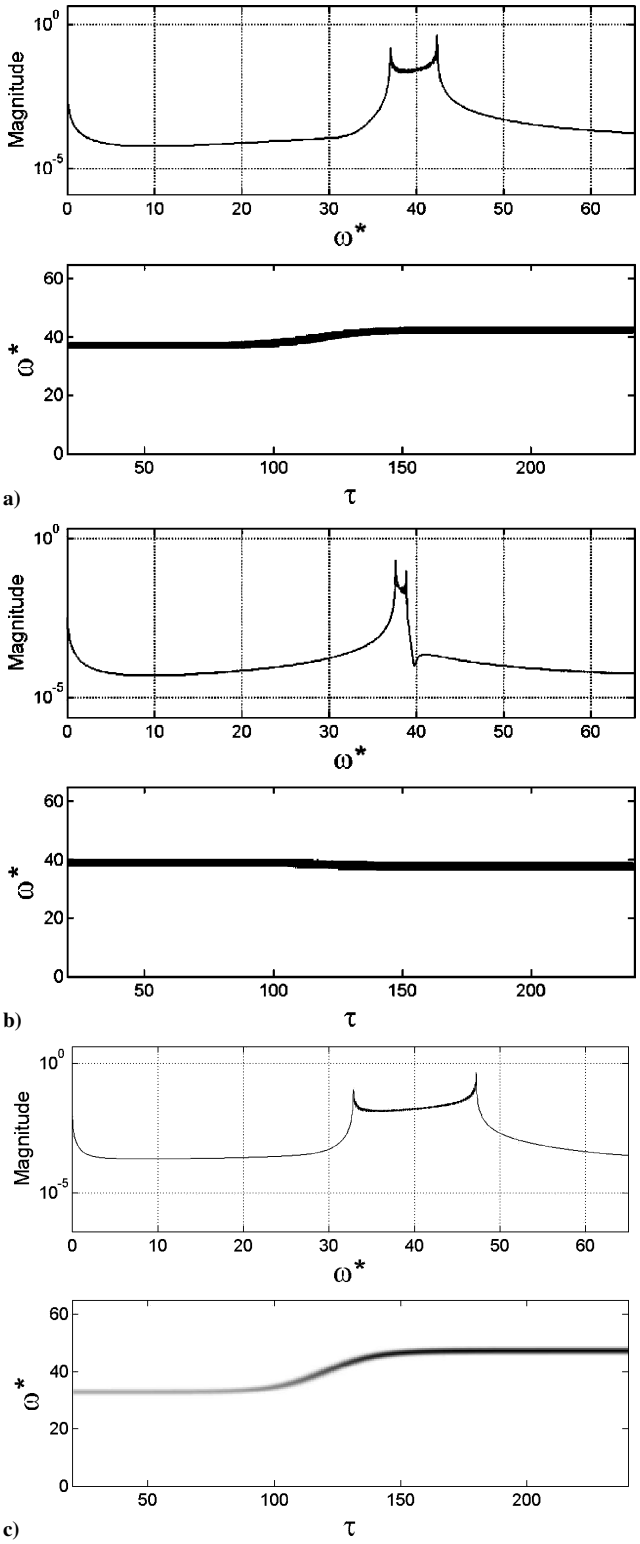

Fig. 11 FFT plots and spectrograms: a) $\lambda = 500$, $\zeta = 0.01$, $\hat{\zeta} = 0.1$, $\bar{N}_0 = 0$; b) $\lambda = 500$, $\zeta = 0.001$, $\hat{\zeta} = 0.1$, $\bar{N}_0 = 0$; and c) $\lambda = 600$, $\zeta = 0.03$, $\hat{\zeta} = 0.1$, $\bar{N}_0 = 0$.

stochastic forced oscillations because of turbulence under which several modes are excited. In this section we consider randomness in the in-plane loading and in the pressure differential. The influence of each type will be examined separately.

In Eqs. (15) the in-plane loading $\bar{N}_{x0}(\tau)$ and pressure differential $\bar{p}_0(\tau)$ will be represented by a mean value superimposed with a random component, that is, $\bar{N}_{x0}(\tau) = \bar{N}_0 + N_x(\tau)$, and $\bar{p}_0(\tau) = \bar{p}_0 + p(\tau)$, where $N_x(\tau)$ and $p(\tau)$ are independent Gaussian wide-band random processes with zero means and delta correlation functions

$$R_N(\Delta\tau) = E[N_x(\tau)N_x(\tau + \Delta\tau)] = S_N\delta(\Delta\tau) \tag{23a}$$

$$R_p(\Delta\tau) = E[p(\tau)p(\tau + \Delta\tau)] = S_p\delta(\Delta\tau) \tag{23b}$$

that is, they are Gaussian white-noise processes with spectral density levels S_N and S_p, respectively, and $\delta(\Delta\tau)$ is the Dirac-delta function. The white-noise processes $N_x(\tau)$ and $p(\tau)$ can be expressed as the formal derivative of the Brownian motions[19]

$$N_x(\tau) = \sigma_N \frac{\mathrm{d}B_N(\tau)}{\mathrm{d}\tau} \tag{24a}$$

$$p(\tau) = \sigma_p \frac{\mathrm{d}B_p(\tau)}{\mathrm{d}\tau} \tag{24b}$$

In this case, Eqs. (15) can be written in terms of Itô stochastic integrals. Through the coordinate transformation $\{q_1, q_1, q_2, q_2\} = \{X_1, X_2, X_3, X_4\} = \boldsymbol{X}$, Eqs. (15) take the Itô form

$$\mathrm{d}X_i(\tau) = f_i(\boldsymbol{X}, \tau)\,\mathrm{d}\tau + \sum_{j=1}^{m} G_{ij}(\boldsymbol{X}, \tau)\,\mathrm{d}B_j(\tau), \qquad i = 1, 2, 3, 4 \tag{25}$$

Although the response coordinate vector $\boldsymbol{X}$ constitutes a Markov process, it is not possible to derive a closed-form solution of the corresponding Fokker–Planck equation.[19] Because of the parametric excitation term in the in-plane loading term $N_x(\tau)$, the moment closure schemes will not give reliable results. Owing to the nonstationarity of the panel response, it is convenient to carry out Monte Carlo simulation[20] to estimate the response mean squares. The time-history records will be processed to determine the autocorrelation function in order to determine the response power spectra and spectrograms.

Influence of in-Plane Random Loading

Under random in-plane loading and constant differential pressure the stability boundary in the (S_N, z) plane is estimated for three different values of dynamic pressure below the critical value, that is, $\lambda < \lambda_{cr}$. The stability boundaries shown in Fig. 12 reveal that as the dynamic pressure increases, to any value below the critical value, the panel becomes more stable. This means that the airflow provides an additional damping to the panel to stabilize it. The dependence of the first-mode mean square response on the in-plane power spectral density for zero dynamic pressure is shown in Fig. 13a for different values of relaxation parameter z. It is seen that the bifurcation point for the case of nearly clamped–clamped boundaries ($z = 0.001$) occurs at a larger value of in-plane load level than the case of the near

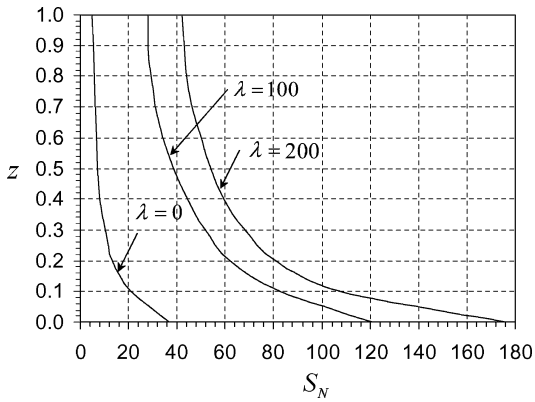

Fig. 12 Stochastic stability boundaries under in-plane random excitation for different values of dynamic pressure parameter λ and system parameters $\bar{p}_0 = 0$, $\zeta = 0.001$, $\hat{\zeta} = 0.1$, $\bar{N}_0 = 0$.

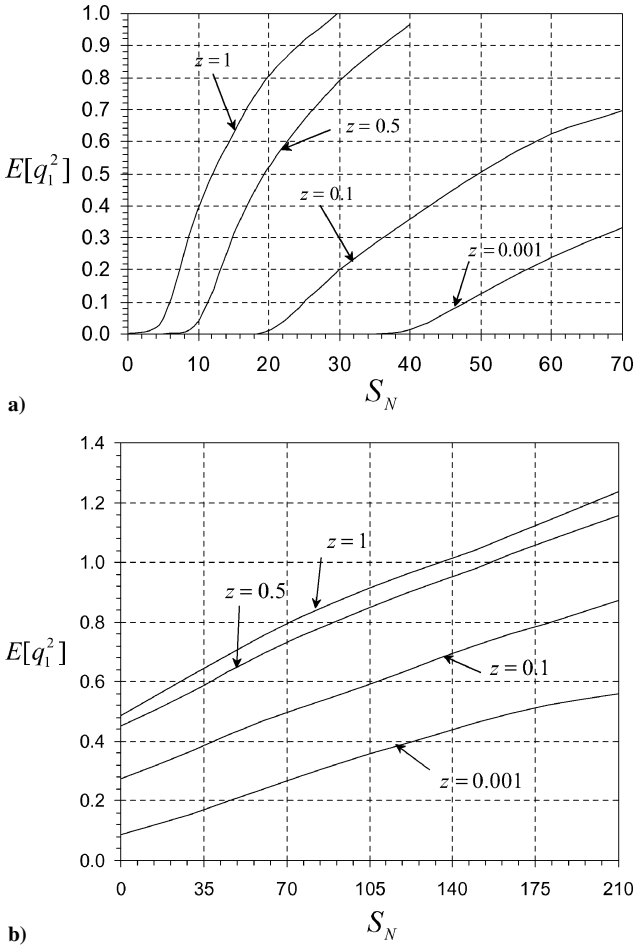

Fig. 13 Dependence of first-mode mean square response on in-plane power spectral density level for different values of relaxation parameter z and $\zeta = 0.001$, $\hat{\zeta} = 0.1$, $\bar{p}_0 = \bar{N}_0 = 0$: a) $\lambda = 0$ and b) $\lambda = 500$.

simply–simply supported panel ($z = 1$). This trend is maintained for any value of dynamic pressure $\lambda < \lambda_{cr}$. For $\lambda > \lambda_{cr}$, the bifurcation point disappears, and the panel possesses a nonzero mean square response at zero in-plane level as shown in Fig. 13b for $\lambda = 500$. At $S_N = 0$, the value of the response mean square increases as the boundary conditions approach the nearly simply supported case.

The time-history records of the panel first-mode displacement and its mean square are shown in Figs. 14a and 14b, respectively, for $\lambda = 500$ and in-plane spectral density $S_N = 40$. Monte Carlo simulation was carried out for an ensemble of 250 excitation samples, and the response statistics were determined in the time and frequency domains. The estimated mean square responses reveal nonstationarity during relaxation, but the nonstationarity diminishes before and after relaxation. The power spectra and spectrograms were estimated for two different damping values $\xi = 0.001$ and 0.01 (Figs. 15a and 15b, respectively). It is seen that for very small damping both structural nonlinearity and relaxation of boundary conditions compensate each other, and the variation of the frequency content is very small. By increasing the damping factor, the structure nonlinearity overcomes the influence of relaxation, and the frequency content increases as the boundary conditions become nearly simply supported.

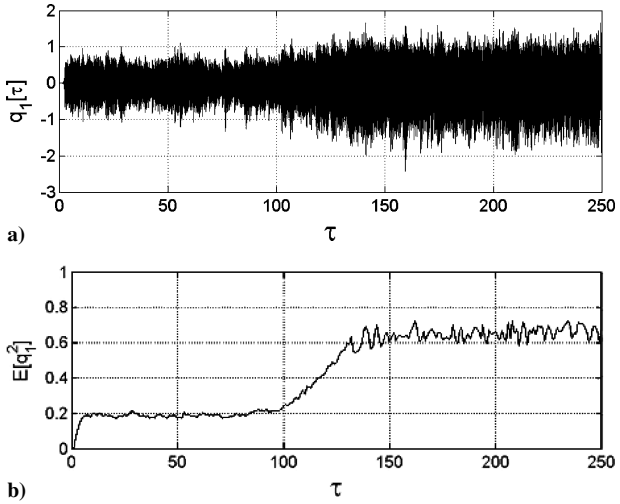

Fig. 14 Time-history records of first-mode a) amplitude and b) its mean square under in-plane random excitation for $\lambda = 500$, $\zeta = 0.001$, $\hat{\zeta} = 0.1$, $\bar{p}_0 = 1$, $\bar{N}_0 = 0$, and $S_N = 40$.

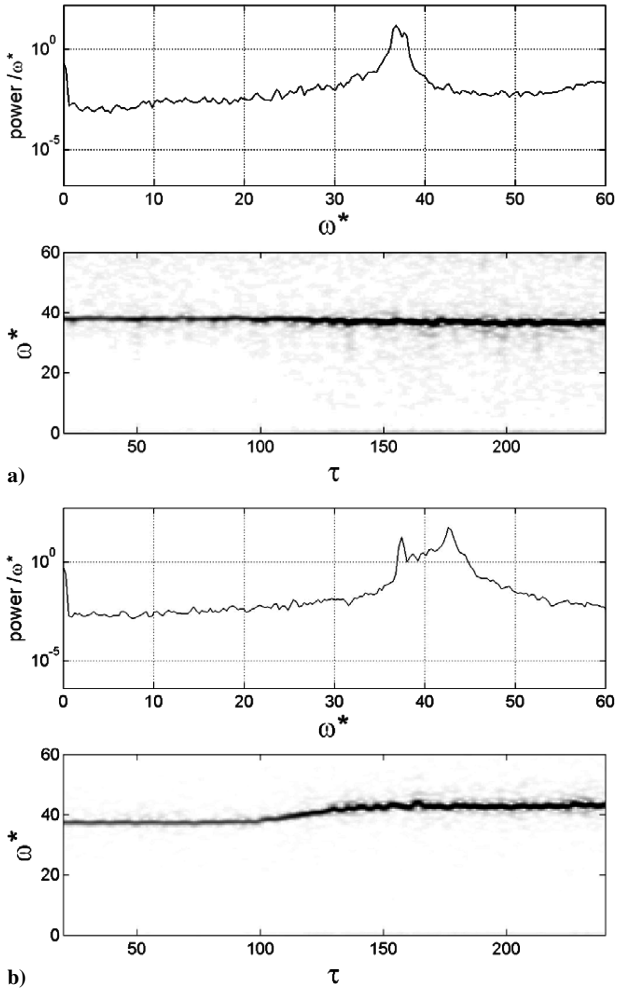

Fig. 15 Power spectra and spectrograms for $\lambda = 500$, $\hat{\zeta} = 0.1$, $\bar{p}_0 = 1$, $\bar{N}_0 = 0$, and $S_N = 40$: a) $\zeta = 0.001$ and b) $\zeta = 0.01$.

Influence of Random Pressure Differential

Under random pressure differential the mean square responses of the panel modes are nonlinearly proportional to the spectral density of the pressure. However, careful inspection of Figs. 16a and 16b reveals that for small excitation level the mean squares are linearly proportional to the excitation spectral density. This is true for all values of relaxation parameter z and dynamic pressures below the critical value $\lambda < \lambda_{cr}$. Note that for $\lambda = 100$ the mean square response is significantly reduced from its value at $\lambda = 0$ because of the aerodynamic damping. Above the critical value of dynamic pressure, that is, $\lambda > \lambda_{cr}$, the mean square response is nonzero at zero random pressure because the panel LCO takes place, as shown in Fig. 16c. Figure 17 shows the reversal effect of the dynamic pressure for $\lambda < \lambda_{cr}$, where mean square response decreases with the excitation, and $\lambda > \lambda_{cr}$, where the opposite is true.

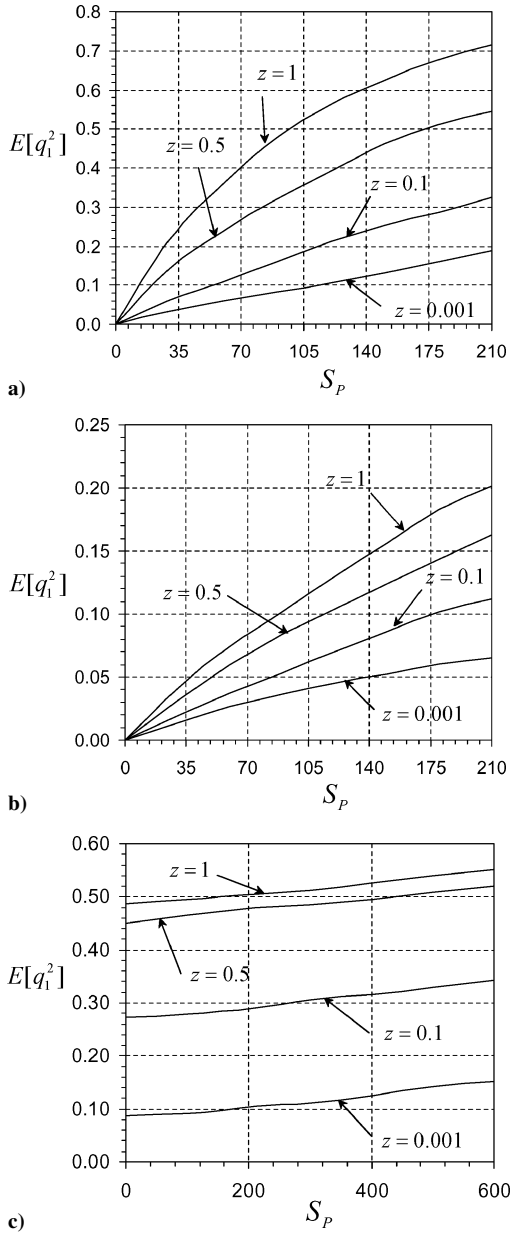

Fig. 16 Dependence of first-mode mean square response on pressure differential power spectral density level for different values of relaxation parameter z and $\zeta = 0.001$, $\hat{\zeta} = 0.1$, $\bar{p}_0 = \bar{N}_0 = 0$: a) $\lambda = 0$, b) $\lambda = 100$, and c) $\lambda = 500$.

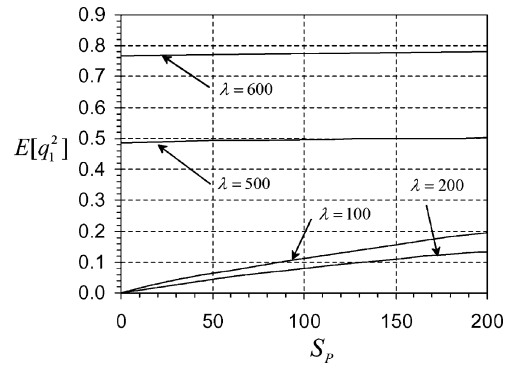

Fig. 17 Dependence of first-mode mean square response on pressure differential power spectral density level for different values of dynamic pressure parameter below and above the critical value λ_{cr} and for $\zeta = 0.001$, $\hat{\zeta} = 0.1$, $\bar{p}_0 = \bar{N}_0 = 0$, and $z = 1$.

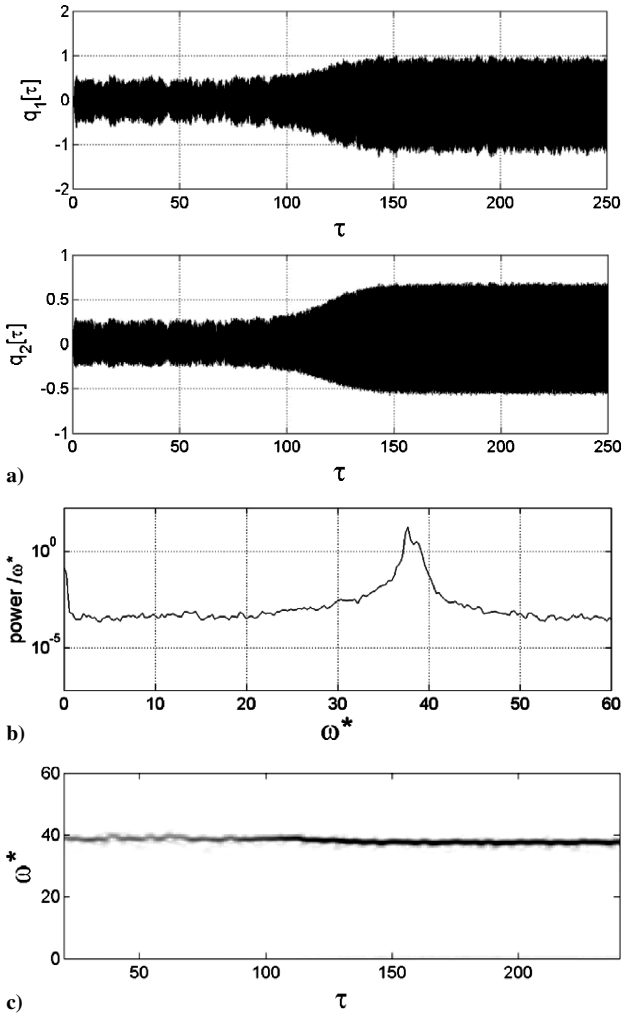

Fig. 18 Time, frequency, and time-frequency domains of panel flutter: a) time-history records of panel first two modes under random pressure differential b) power spectral density and c) spectrogram of the panel first mode under random pressure differential for $\zeta = 0.001$, $\hat{\zeta} = 0.1$, $\bar{p}_0 = 1$, $\bar{N}_0 = 0$, $\lambda = 500$, and $S_p = 40$.

Figure 18a shows the time-history records of the two modes under excitation spectral density $S_p = 40$ and dynamic pressure $\lambda = 500 > \lambda_{cr}$. It is seen that the first mode exhibits more randomness than the second mode because the first mode acts as a nonlinear filter to the second mode as revealed from the two modal equations (15). Figures 18b and 18c show the corresponding response power spectral density and spectrogram for the first mode.

Conclusions

The influence of boundary conditions relaxation on a two-dimensional panel flutter has been studied under deterministic and random conditions. The panel flutter is studied in terms of the first two modes whose eigenvalues are estimated based on the linear modal differential equations. The real value of the eigenvalues determines the critical flutter speed, and it is found that the relaxation of the boundary conditions reduces the value of the flutter speed. The dependence of the natural frequencies (the imaginary parts) on relaxation parameter for different values of aerodynamic pressure revealed a drop in the natural frequencies with relaxation and an increase with dynamic pressure for the first mode. However, the second-mode natural frequency decreases with dynamic pressure. The boundaries of panel flutter are obtained in terms of in-plane load, relaxation parameter, and damping factor. The damping of the panel exhibits a critical value governed by the relaxation parameter, below which the damping has a destabilizing effect and above which it has stabilizing effect. The dependence of the LCO amplitude on dynamic pressure is obtained for different values of

relaxation parameter and is found to be bounded between the two limiting cases of simply supported and clamped–supported boundary conditions. The amplitude time-history records reveal an increase in the modal amplitudes after the end of relaxation because the boundary conditions are nearly simply supported. However, the frequency content is governed by the relaxation, geometric nonlinearity, and damping. There is a competition among these three parameters, which can the frequency content to either increase or decrease with time.

Under random in-plane loading, the stochastic mean square stability boundaries are obtained for dynamic pressures that are below the critical flutter value. As the dynamic pressure increases, but still below the critical value, the stability region is enlarged because of aerodynamic damping. Above the critical value the panel modes achieve random LCO whose mean square is nonzero under zero in-plane excitation. The time-history records display nonstationary random fluctuations during the relaxation process, and the scatter is persistent before and after relaxation. Under random pressure differential the first mode exhibits more nonstationarity than the second mode because the first mode acts as a nonlinear filter to the second mode.

Acknowledgments

This research is supported by grants from the Institute for Manufacturing Research and the Air Force Office of Scientific Research (AFOSR) under Grant F49620-03-1-0229. Dean Mook is the AFOSR Program Director.

References

[1]Dowell, E. H., *Aeroelasticity of Plates and Shells*, Noordhoff, Leyden, The Netherlands, 1985.

[2]Dowell, E. H., "Flutter of a Buckled Plate as an Example of Chaotic Motion of a Deterministic Autonomous System," *Journal of Sound and Vibration*, Vol. 85, No. 3, 1982, pp. 333–344.

[3]Fung, Y. C., "Some Recent Contributions to Panel Flutter Research," *AIAA Journal*, Vol. 1, No. 4, 1963, pp. 898–909.

[4]Eastep, F. E., and McIntosh, S. C., Jr., "Analysis of Nonlinear Panel Flutter and Response Under Random Excitation or Nonlinear Aerodynamic Loading," *AIAA Journal*, Vol. 9, No. 3, 1971, pp. 411–418.

[5]Vaicaitis, R., Dowell, E. H., and Ventres, C. S., "Nonlinear Panel Response by a Monte Carlo Approach," *AIAA Journal*, Vol. 12, No. 5, 1974, pp. 685–691.

[6]Tack, D. H., and Lambert, R. F., "Response of Bars and Plates to Boundary Layer Turbulence," *Journal of Aeronautical Sciences*, Vol. 29, No. 3, 1962, pp. 311–322.

[7]Olson, M. D., "Some Flutter Solutions Using Finite Elements," *AIAA Journal*, Vol. 8, No. 4, 1970, pp. 747–752.

[8]Mei, C., "A Finite-Element Approach for Nonlinear Panel Flutter," *AIAA Journal*, Vol. 5, No. 8, 1977, pp. 1107–1110.

[9]Vaicaitis, R., Jan, C. M., and Shinozuka, M., "Nonlinear Panel Response from a Turbulent Boundary Layer," *AIAA Journal*, Vol. 10, No. 7, 1972, pp. 895–899.

[10]Ibrahim, R. A., Orono, P. O., and Madaboosi, S. R., "Stochastic Flutter of a Panel Subjected to Random in-Plane Forces, Part I: Two Mode Interaction," *AIAA Journal*, Vol. 28, No. 4, 1990, pp. 694–702.

[11]Ibrahim, R. A., and Orono, P. O., "Stochastic Nonlinear Flutter of a Panel Subjected to a Random in-Plane Forces," *International Journal for Nonlinear Mechanics*, Vol. 26, No. 6, 1991, pp. 867–883.

[12]Ibrahim, R. A., and Pettit, C. L., "Uncertainties and Dynamic Problems of Bolted Joints and Other Fasteners," *Journal of Sound and Vibration*, Vol. 279, No. 3/4, 2005, pp. 857–936.

[13]Poiron, B., "Impact of Random Uncertainties on Aircraft Aeroelastic Stability," *Proceedings of the Stochastic Structural Dynamics Conference*, San Juan, PR, 1995.

[14]Lindsley, N. J., Beran, P. S., and Pettit, C. L., "Effects of Uncertainty on Nonlinear Plate Response in Supersonic Flow," AIAA Paper 2002-5600, 2002.

[15]Lindsley, N. J., Beran, P. S., and Pettit, C. L., "Effects of Uncertainty on Nonlinear Plate Aeroelastic Response," AIAA Paper 2002-1271, 2002.

[16]Ibrahim, R. A., Beloiu, D. M., and Pettit, C. L., "Influence of Boundary Conditions Relaxation on Panel Flutter," *Proceedings of the IUTAM Symposium on Chaotic Dynamics and Control Systems Processes in Mechanics*, edited by G. Rega and F. Vestroni, Springer, Dordrecht, The Netherlands, 2005, pp. 223–232.

[17]Qiao, S., Pilipchuk, V. N., and Ibrahim, R. A., "Modeling and Simulation of Elastic Structures with Parameter Uncertainties and Relaxation of Joints," *Journal of Vibration and Acoustics*, Vol. 123, No. 1, 2000, pp. 45–52.

[18]Bickford, J. H., *An Introduction to the Design and Behavior of Bolted Joints*, 2nd ed., Marcel Dekker, New York, 1990.

[19]Ibrahim, R. A., *Parametric Random Vibration*, Wiley, New York, 1985.

[20]Shinozuka, M., and Jan, C.-M., "Digital Simulation of Random Processes and Its Applications," *Journal of Sound and Vibration*, Vol. 25, No. 1, 1972, pp. 111–128.

B. Balachandran
Associate Editor